



HAL
open science

Excitonic properties of semiconducting monolayer and bilayer MoT e 2

Cédric Robert, R. Picard, David Lagarde, Gang Wang, J. Echeverry, Fabian Cadiz, Pierre Renucci, A. Högele, Thierry Amand, Xavier Marie, et al.

► **To cite this version:**

Cédric Robert, R. Picard, David Lagarde, Gang Wang, J. Echeverry, et al.. Excitonic properties of semiconducting monolayer and bilayer MoT e 2. *Physical Review B: Condensed Matter and Materials Physics* (1998-2015), 2016, 94 (15), 10.1103/physrevb.94.155425 . hal-01968908

HAL Id: hal-01968908

<https://hal.insa-toulouse.fr/hal-01968908>

Submitted on 14 Jan 2019

HAL is a multi-disciplinary open access archive for the deposit and dissemination of scientific research documents, whether they are published or not. The documents may come from teaching and research institutions in France or abroad, or from public or private research centers.

L'archive ouverte pluridisciplinaire **HAL**, est destinée au dépôt et à la diffusion de documents scientifiques de niveau recherche, publiés ou non, émanant des établissements d'enseignement et de recherche français ou étrangers, des laboratoires publics ou privés.

Excitonic properties of semiconducting monolayer and bilayer MoTe₂C. Robert,^{1,*} R. Picard,¹ D. Lagarde,¹ G. Wang,¹ J. P. Echeverry,¹ F. Cadiz,¹ P. Renucci,¹ A. Högele,² T. Amand,¹ X. Marie,¹ I. C. Gerber,^{1,†} and B. Urbaszek¹¹*Université de Toulouse, INSA-CNRS-UPS, LPCNO, 135 Avenue de Rangueil, 31077 Toulouse, France*²*Fakultät für Physik, Center for NanoScience (CeNS), Ludwig-Maximilians-Universität München, Geschwister-Scholl-Platz 1, 80539 München, Germany, EU*

(Received 10 June 2016; revised manuscript received 22 September 2016; published 17 October 2016)

MoTe₂ belongs to the semiconducting transition-metal dichalcogenide family with certain properties differing from the other well-studied members (Mo,W)(S,Se)₂. The optical band gap is in the near-infrared region, and both monolayers and bilayers may have a direct optical band gap. We first simulate the single-particle band structure of both monolayer and bilayer MoTe₂ with density-functional-theory-*GW* calculations. We find a direct (indirect) electronic band gap for the monolayer (bilayer). By solving in addition the Bethe-Salpeter equation, we find similar energies for the direct exciton transitions in monolayers and bilayers. We then study the optical properties by means of photoluminescence (PL) excitation, reflectivity, time-resolved PL, and power-dependent PL spectroscopy. With differential reflectivity, we find a similar oscillator strength for the optical transition observed in PL in both monolayers and bilayers suggesting a direct transition in both cases. We identify the same energy for the *B*-exciton state in the monolayer and the bilayer. Following circularly polarized excitation, we do not find any exciton polarization for a large range of excitation energies. At low temperatures ($T = 10$ K), we measure similar PL decay times on the order of 4 ps for both monolayer and bilayer excitons with a slightly longer one for the bilayer. Finally, we observe a reduction of the exciton-exciton annihilation contribution to the nonradiative recombination in bilayers.

DOI: [10.1103/PhysRevB.94.155425](https://doi.org/10.1103/PhysRevB.94.155425)**I. INTRODUCTION**

Monolayers (MLs) of group-VI transition-metal dichalcogenide (TMD) form a new class of semiconducting materials with exciting properties for electronics and optoelectronics applications [1–4]. MoS₂ was the first studied material [5,6] quickly followed by extensive studies on binary WS₂, MoSe₂, WSe₂ [7,8], and ternary alloys [9–11]. In the 2*H* hexagonal structure, these materials all share common properties: (i) an indirect-to-direct band-gap crossover when the material is thinned down to the monolayer limit [5,6] where the direct gap is located at the K^\pm points of the hexagonal Brillouin zone, (ii) strong binding energies for excitons (Coulomb bound electron-hole pairs) of several hundreds of meV [12–14], and (iii) spin- and valley-dependent optical selection rules due to the lack of crystal inversion symmetry and large spin-orbit coupling (SOC) [15–19]. Nevertheless, several differences in the physical properties between semiconducting TMD MLs materials can be pointed out. The amplitude of the valence spin-orbit splitting varies from less than 200 meV for Mo(S,Se)₂ MLs to more than 400 meV for W(S,Se)₂ MLs. The sign of the splitting between intravalley bright and dark excitons is the opposite in MoSe₂ and WSe₂ MLs [20], dramatically affecting their optical properties [11,21,22]. Finally, despite comparable structural and optical qualities, the valley-/spin-polarization properties probed in optical spectroscopy are very different between materials. For MoS₂ MLs, the degree of circular polarization of the photoluminescence (PL) decreases monotonously when the detuning of the excitation laser energy relative to the

excitonic ground state increases [23,24]. For WSe₂ and WS₂ MLs, circularly polarized PL has been reported even for excitation energies far from the resonance, but the polarization degree is exalted for excitation energies in resonance with exciton excited states ($2s$ or $2p$) [14,25]. In contrast, no PL polarization has been observed in MoSe₂ MLs except for quasiresonant excitation [24].

Recently, the family of semiconducting TMD monolayers expanded with a fifth binary material: MoTe₂ [26,27]. Two striking properties have been highlighted by the first studies on this material: The optical band gap of MoTe₂ MLs is in the near infrared (IR) (1.1 eV at room temperature [26]) whereas it lies in the red part of the visible spectrum for S- and Se-based compounds. Second, the luminescence yield of MoTe₂ bilayers (BLs) is on the same order of magnitude as the luminescence yield of the ML opening a debate on a possible direct band gap for BLs [27,28]. Nevertheless, the high luminescence yield of BLs is up to now the only argument pointing towards a direct band gap. In addition, many properties, such as radiative lifetime, spin/valley polarization, and the energy of exciton excited states, have not been measured in this material yet. In this paper we partially fill this gap by studying theoretically and experimentally the optical properties of both MoTe₂ MLs and BLs. The paper is organized as follows. In the next section, we use DFT + *GW* calculations to simulate the band structures of both the ML and the BL in a single-particle picture (no excitonic effects). Remarkably we find an indirect electronic band gap for the BL. We then solve the Bethe-Salpeter equation (BSE) to include the strong electron-hole Coulomb attraction when calculating the energy and the oscillator strength of direct excitonic transitions. Section III is dedicated to stationary PL measurements. Experimentally, we measure the splitting between *A* and *B* excitons by PL excitation spectroscopy

*cedric.robert@insa-toulouse.fr

†igerber@insa-toulouse.fr

and reflectivity and compare the results with $G_0W_0 + \text{BSE}$ calculations. We do not find any Stokes shift between the PL of the A exciton and the strong signature observed in reflectivity in both the ML and the BL indicates a direct optical band gap in both systems. We also do not detect any measurable PL polarization for excitation energy as close as 60 meV above the energy of the A exciton suggesting a behavior similar to MoSe_2 MLs. In Sec. IV, we use time-resolved PL to measure the exciton lifetime in the range of a few picoseconds in both MLs and BLs with a slightly longer one for BLs. Finally, in Sec. V, we show that exciton-exciton annihilation (EEA) is larger in MLs than in BLs.

II. ELECTRONIC BAND-STRUCTURE CALCULATION

In recent years, DFT + GW methods have been successfully applied to calculate the electronic band gap of two-dimensional (2D) semiconductor materials (E_G), see, for instance, Refs. [14,29–32]. In the present paper, the exploration of the electronic structure and optical properties of ML and BL MoTe_2 has been performed using the VASP code [33,34]. It uses the plane-augmented-wave scheme [35,36] to treat core electrons when 14 electrons for Mo and 6 for Te ones are explicitly included in the valence states with a plane-wave energy cutoff of 400 eV. The Heyd-Scuseria-Ernzerhof hybrid functional [37–39] is used to build the needed wave functions, based on 600 electronic states, to calculate the full-frequency-dependent quasiparticle band structure at the G_0W_0 level of theory [40], including SOC but not the excitonic effects at this stage. This particular choice of the computational settings has been discussed in detail in Ref. [20]. A grid of $(12 \times 12 \times 1)k$ points has been used in conjunction with a vacuum height of at least 17 Å for both the ML and the BL systems. For the latter, we have selected the stacking geometry of AA' type since it appears to be the most stable BL structure [41]. It corresponds to the point-group D_{3d} symmetry with an eclipsed stacking with Mo over Te. The optimized interlayer distance is 7.00 Å when van der Waals (VdW) forces are taken into account via the optB86b-VdW scheme [42].

In Fig. 1(a), the resulting DFT + G_0W_0 band structure of the MoTe_2 ML is shown after a Wannier interpolation procedure performed by the WANNIER90 program [43]. Its main features agree well with previous theoretical studies [29,44]. It has a direct electronic band gap in the K valley with a value of 1.72 eV, a SOC splitting in the valence band of 275 meV whereas it is -58 meV in the conduction band. The negative sign for the conduction band SOC means that both conduction-band minimum and valence band maximum have the same spin, i.e., the lowest-lying interband transition is bright. In comparison the BL band structure at the same level of theory is given in Fig. 1(b). If the direct K_V-K_C gap remains almost the same with a value of 1.66 eV for the BL, now it appears that the indirect $K_V-\Lambda_C$ quasiparticle band gap is the lowest one with a value of 1.60 eV. Thus the interlayer interaction leads to a transition from a direct to an indirect band gap similar to other group-VI TMDs [41] with an energy separation between K_C and Λ_C remaining small compared to other TMD systems. Nevertheless, contrary to MoS_2 BLs, the valence-band minimum remains in the K valley [41]. The interlayer interaction also tends to enhance the energy separation between the two

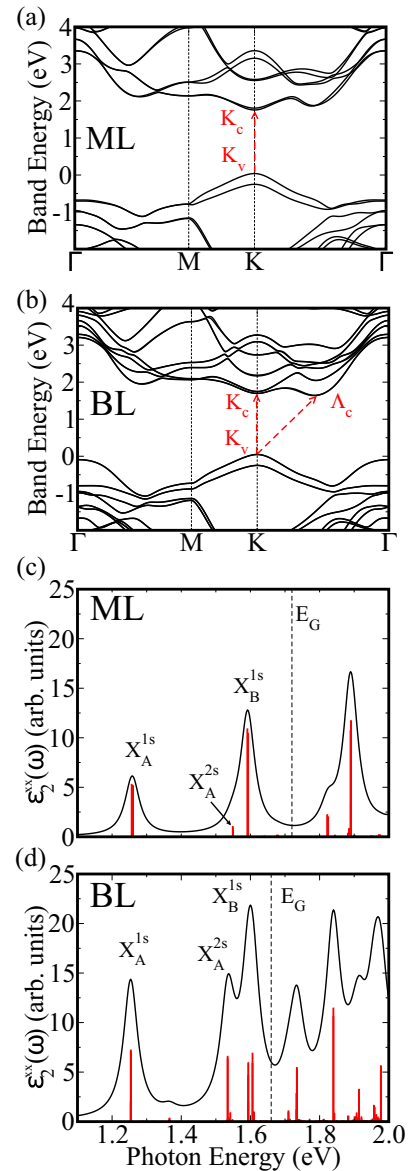


FIG. 1. Quasiparticle band structure for a freestanding MoTe_2 (a) ML and (b) BL, at the G_0W_0 level of theory, extracted from a Wannier localization procedure. The energy at the valence-band maximum (in K) is set to zero for the sake of comparison. The imaginary part of the transverse dielectric constant $\epsilon_2^{xx}(\omega)$ as a function of photon energy (in eV) for the MoTe_2 (c) ML and (d) BL. The red bars represent the relative oscillator strengths for the optical transitions, whereas the dashed line indicates the G_0W_0 band gap.

highest valence states of different spins for each layer, whereas the opposite is true for the lowest unoccupied ones. As a result, the SOC splittings become 304 and -46 meV for the valence and conduction bands, respectively.

With DFT + GW calculations we find that the electronic band gap is direct for the ML and indirect for the BL. But in TMD materials, the optical properties are not governed by the band-to-band recombination. In reality, due to the very large exciton binding energy ($E_B \sim 500$ meV), the PL spectrum is dominated by the ground exciton transition (also called optical band-gap $E_{\text{PL}} = E_G - E_B$). To calculate the optical band gap,

we need to include the electron-hole Coulomb interaction into the model by solving the BSE. Practically BSE spectra are obtained in the Tamm-Dancoff approximation by using the six highest valence bands and the eight lowest conduction bands for the MoTe₂ ML and 12 valence and 16 conduction bands for the BL to obtain eigenvalues and oscillator strengths with a complex shift of 25 meV to broaden the theoretical absorption spectra. Although absorption and PL probe different physical processes, the calculation of the absorption spectrum can help to identify features, such as *A-B* and *1s-2s* splittings [14,32]. Only direct transitions are taken into account in this calculation. For TMD MLs, this is assumed to give a correct description of the main excitonic states as both electronic and optical band gaps are direct. But for MoTe₂ BLs for which we find an indirect electronic band gap, we would need to add the exciton-phonon interaction into the scheme to draw conclusions on the indirect-direct nature of the optical band gap. Unfortunately this refinement is not trivial and is far beyond the scope of this paper [45].

The BSE spectra are given in Figs. 1(c) and 1(d). We can identify in both spectra the ground states of both *A* and *B* excitons (namely, X_A^{1s} and X_B^{1s}). Interestingly the position of the X_A^{1s} and X_B^{1s} peaks remains at the same energy when going from the ML to the BL. The corresponding binding energy is thus 0.46 eV for the *A* exciton in the ML and 0.4 eV in the BL. We recall that the exciton binding energy is defined as the energy difference between the smallest direct band gap, here at the *K* point, and the first optical transition energy. The BL exciton binding energy is slightly larger than the values obtained on other Mo-based TMDs for which typical values are lower than 0.3 eV [41,46]. This could be a direct consequence of: (i) the larger interlayer distance when passing from S to Te composition and (ii) of a weaker intralayer screening for MoTe₂, which reduces significantly the binding energy at the ML level already. To go further in the evolution of E_B with respect to the number of layers, we have calculated the band structure and the absorption spectrum for the MoTe₂ bulk system. Our calculation suggests that the decrease in E_B when increasing the number of layers is system dependent. For MoTe₂, the direct band gap evolves from 1.72 to 1.46 eV when passing from ML to bulk. This decrease is less pronounced than in MoS₂ and MoSe₂ systems where the direct band gap in *K* is reduced by more than 30% [46]. We also observe this trend for exciton binding energy values. We have obtained a binding energy for bulk MoTe₂ of around 0.16 eV, in good agreement with an experimental determination reported in Ref. [47]. So the ratio between bulk and ML exciton binding energies is around 33%, whereas for MoS₂ it is on the order of 20% if one considers roughly the exciton ML binding energy around 0.5 and 0.1 eV for the bulk.

From the ML spectrum we can also identify a small shoulder at 0.04 eV below the X_B^{1s} peak, which can be safely assigned to a transition associated with the *2s* state of the *A* exciton. Indeed this transition appears as soon as the *A* states are included in the valence-band subset of the BSE matrix. This peak is also present in the BL spectrum, but it is slightly shifted by 0.01 eV to lower energy. Another interesting feature is the extra peak located at 0.01 eV above the X_A^{1s} peak when stacking the two layers. This transition has non-negligible oscillator strength and is of interlayer character. Indeed it involves the fifth and

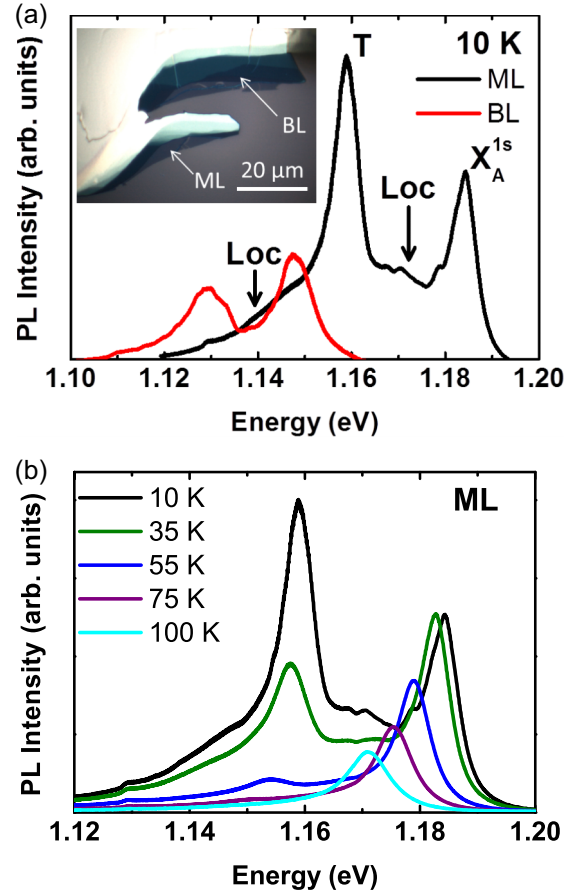


FIG. 2. (a) PL spectra of the MoTe₂ ML (black) and BL (red) at 10 K. The inset: optical microscope image used for the identification of ML and BL regions. (b) PL spectra of the MoTe₂ ML from 10 to 100 K. The sample is excited with a cw HeNe laser (633 nm) at a power of 50 μ W.

sixth conduction bands which clearly possess a delocalized character over the two layers and is composed mainly of d_{xz} and d_{yz} orbitals of the two Mo atoms. Note that this kind of weak interlayer transition in the vicinity of the *A* peak has been previously reported not only in the case of the MoS₂/WS₂ heterostructure [30], but also for bilayers [41].

III. CONTINUOUS-WAVE SPECTROSCOPY

Our DFT calculations predict at the *GW* level a direct gap for the ML and an indirect gap for the BL with a direct gap only 60 meV above in energy. This energy difference is very small once excitonic effects (\sim 500 meV) are taken into account. This motivates the optical spectroscopy studies described in this section where ML and BL emission energies and intensities can be determined.

For experimental studies of optical properties, we use MoTe₂ flakes obtained by micromechanical cleavage of a bulk MoTe₂ crystal (supplied by the company 2D semiconductors) on a 90-nm SiO₂/Si substrate using viscoelastic stamping [48]. For reflectivity measurements, we use transparent quartz substrates. The ML and BL regions are identified by optical contrast [see the inset of Fig. 2(a)] and very clearly in PL

spectroscopy [Fig. 2(a)]. Experiments between 4 and 300 K are carried out on a confocal microscope optimized for polarized PL experiments in the near IR. After dispersion with a near-IR blazed grating, the PL is analyzed with an InGaAs photodiode array for continuous-wave (cw) experiments or a S1 photocathode streak camera (Hamamatsu C5680) for time-resolved photoluminescence (TRPL) measurements. For cw excitation, three different lasers are used. A standard HeNe laser is used for strongly nonresonant excitation whereas a cw Ti:sapphire laser and a tunable laser diode are used to adjust the excitation wavelength from 750 to 1000 nm. For TRPL measurements, we excite the sample with 1.5-ps pulses of a Ti:sapphire laser at a wavelength of 850 nm and a repetition rate of 80 MHz. For reflectivity measurements, we use a tungsten-halogen lamp. For all measurements, the laser spot diameter is around $1 \mu\text{m}$ on the sample (i.e., much smaller than the flake size), and the average power is set below $100 \mu\text{W}$.

Figure 2(a) presents the low-temperature PL spectra of both ML and BL for an excitation energy above the free carrier gap that we calculate by DFT-GW [Figs. 1(a) and 1(b)]. The spectra are composed of two main peaks typically attributed to the ground states of the neutral exciton X_A^{1s} (at 1.184 eV for the ML) and trion T (at 1.159 eV for a ML) for the A transition. The energies of the peaks are in good agreement with the previously reported PL spectra of MoTe₂ MLs and BLs [26–28]. For the MoTe₂ ML, we measure a separation between the X_A^{1s} and the T peaks of 25 meV in agreement with the measurement of the binding energies of positively and negatively charged excitons in a field effect structure [44] (24 and 27 meV, respectively). For the BL, the separation between peaks is smaller (18 meV), but we cannot unambiguously attribute the low-energy peak to the trion signature as no charge tunable device based on BL has been reported yet. The full width at half maximum is 7 meV for both X_A^{1s} and T in the ML indicating an optical quality as high as for the best MSe₂-(M = Mo, W) ML [49] samples. For comparison, the smallest linewidth at low temperatures we obtained on chemically treated MoS₂ MLs is typically 15 meV [50]. Thus, MoTe₂ is particularly suitable to study the complex exciton/trion fine structure of TMD MLs. Nevertheless, the measured linewidth is still broader than the expected homogeneous linewidth (see also Sec. IV). This indicates that disorder may impact the radiative recombination, the Coulomb interaction, and the spin-orbit coupling properties [51,52]. In addition to the two main peaks we observe features on the low-energy part of the spectrum and between X_A^{1s} and T peaks. We attribute them to complex localized states [marked as Loc in Fig. 2(a)] as their contribution to the PL spectrum vanishes when the temperature increases [see Fig. 2(b)]. We also want to point out that the amplitude of these localized states varies from a ML-to-ML sample making the origin of these features difficult to attribute at this stage.

Several important characteristics of TMD MLs (optical generation of valley polarization, second-harmonic generation efficiency) are known to strongly depend on the laser excitation energy as the light-matter interaction is strongly enhanced at the excitonic resonances [14,24,53,54]. Therefore, probing the excited excitonic states is of particular importance. Figure 3(a) presents the PL excitation (PLE) spectra corresponding to the variation of the X_A^{1s} PL intensity as a function of the

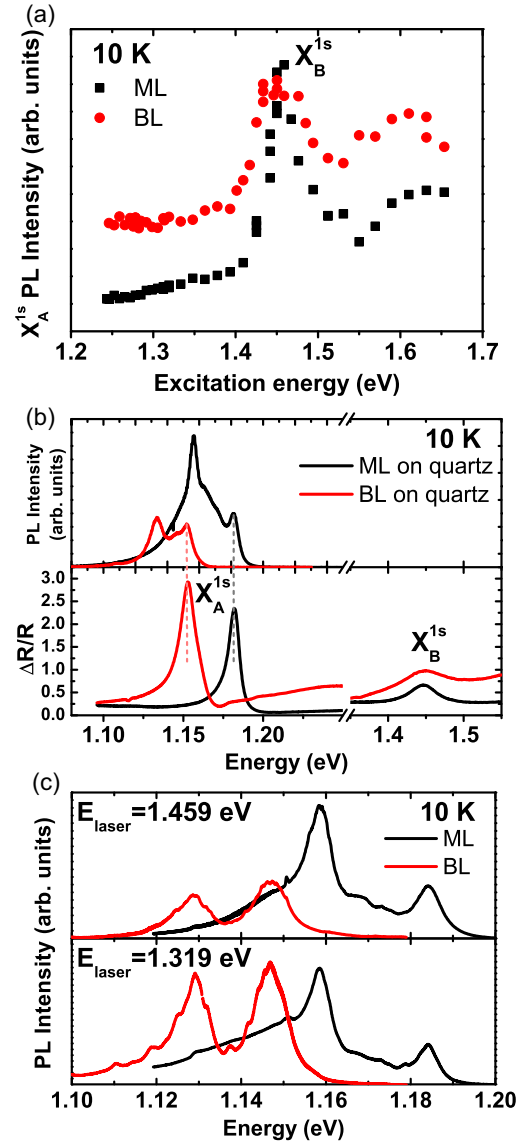


FIG. 3. (a) PLE spectra (PL intensity of the X_A^{1s} peak as a function of excitation energy) of the MoTe₂ ML (black square points) and BL (red circle points) at 10 K. The sample is excited with a cw Ti:sapphire laser for wavelengths between 750 nm (1.65 eV) and 950 nm (1.31 eV) and with a tunable laser diode for wavelengths between 950 nm (1.31 eV) and 1000 nm (1.24 eV). The laser power is $50 \mu\text{W}$. (b) PL spectra of the MoTe₂ ML (black) and BL (red) at 10 K on a quartz substrate (top panel) and differential reflectivity $\Delta R/R = (R_{\text{flake}} - R_{\text{quartz}})/R_{\text{quartz}}$ (bottom panel). For the PL experiment, the sample is excited with a cw HeNe laser (633 nm) at a power of $50 \mu\text{W}$. (c) PL spectra of the MoTe₂ ML (black) and BL (red) at 10 K for two different excitation laser energies. The sample is excited at a power of $50 \mu\text{W}$.

laser energy. The PLE spectra depend on the absorption at the excitation energy and how the carriers relax down to the X_A^{1s} state. A clear resonance of the X_A^{1s} PL peak is observed at 1.45 eV for both the ML and the BL which corresponds to the signature of the ground B exciton state X_B^{1s} . The energy of the X_B^{1s} state is also confirmed in the reflectivity spectrum of Fig. 3(b), which scales like the absorption spectrum without being sensitive to carrier relaxation as the

PLE measurements. We thus find a splitting $B-A$ of 270 meV for the ML in agreement with the room-temperature reflectivity measurement of Ruppert *et al.* (260 meV) [26]. This is also in good agreement with the BSE spectrum of Fig. 1(c) where we calculate a splitting of 330 meV. We notice that this splitting is larger than for the other Mo-based TMDs. Finding exactly the same X_B^{1s} resonance energy for both a ML and a BL (while there is a 35-meV shift for the X_A^{1s} resonance energy) is also interesting and in good agreement with the calculations of Figs. 1(c) and 1(d).

Contrary to measurements on WSe₂ MLs [55], we do not find a clear signature of the X_A^{2s} excited state in the PLE spectrum of the MoTe₂ ML. A possible explanation is that this state is very close to the X_B^{1s} state, such as in MoSe₂ MLs [56] and cannot be distinguished in the PLE spectrum. This is supported by the GW -BSE calculations of Fig. 1(c) where we find a separation $X_B^{1s} - X_A^{2s}$ of 40 meV thus smaller than the width of the PLE peak in Fig. 3(a). Two-photon experiments would be an efficient way to probe the X_A^{2p} state without being sensitive to the X_B^{1s} state [56]. However this requires exciting the ML with energies lower than 0.75 eV, which is beyond the tuning range of conventional laser systems. For the BL we can point out that the resonance peak at 1.45 eV observed in both PLE and reflectivity spectra is clearly broader than in the ML case and could be a sign of the X_A^{2s} contribution.

Using the ratio of integrated BL PL versus ML PL intensity is not sufficient to distinguish between direct and indirect optical transitions. Indeed, the laser energy E_{laser} used for excitation plays an important role as can be seen in Fig. 3(c). For example, the BL PL emission for $E_{\text{laser}} = 1.319$ eV is more intense than the ML PL. A stronger argument is given by the reflectivity spectrum of Fig. 3(b). Because the flakes are transferred onto a thick transparent quartz substrate in this experiment, the differential reflectivity given by $\Delta R/R = (R_{\text{flake}} - R_{\text{quartz}})/R_{\text{quartz}}$ qualitatively resembles the absorption spectrum [57–59]. For both ML and BL samples, a strong resonance in $\Delta R/R$ is observed at the exact energy of the X_A^{1s} PL peak. Remarkably, the strength of this resonance is similar in MLs and BLs. These results are a strong indication that the BL PL transition corresponds to a direct optical gap at this energy.

TMD MLs obey chiral optical interband selection rules [15] that allow for optical excitation in either the K^+ or the K^- valley depending on excitation laser helicity. For the range of excitation energies shown in Fig. 3(a), we do not measure any significant circular (linear) polarization following circularly (linearly) polarized excitation. This behavior is in agreement with the very recent zero polarization reflectivity measured at a zero magnetic field [60]. This is also similar to what was observed for the MoSe₂ ML [23]. Only one recent study reports a circular PL polarization degree of 20% in the MoSe₂ ML for a difference between the laser energy and the energy of the X_A^{1s} emission of $\Delta E = E_{\text{laser}} - E[X_A^{1s}] = 60$ meV [24]. Longitudinal acoustic (LA) phonon-assisted intervalley scattering was proposed as the cause of depolarization in MoSe₂ and MoS₂ MLs [24]. The larger value of the LA phonon for MoS₂ (30 meV) [61] as compared to MoSe₂ (19 meV) [62] would explain why polarization can be observed in MoS₂ for larger ΔE 's. Interestingly, the LA phonon energy of MoTe₂ is even smaller (12 meV) [63] than that of MoSe₂. Thus, only excitation very close to the resonance may initiate valley po-

larization in this material. Unfortunately, for $\Delta E < 60$ meV, a strong Raman-scattering signal is superimposed on the PL signal resulting in unreliable polarization measurements.

IV. TIME-RESOLVED MEASUREMENTS

The exciton binding energy in a MoTe₂ ML can be roughly estimated by taking the difference between the electronic band gap provided by the DFT- GW calculation [1.72 eV, see Fig. 1(a)] and the optical band gap measured in PL [1.18 eV, see Fig. 2(a)]. We find a binding energy of ~ 540 meV in agreement with previous estimation of Yang *et al.* [44]. Such a strong exciton binding energy and the associated strong oscillator strength are very interesting properties for strong light-matter coupling studies in ML TMDs [64,65]. Consequently, a short PL emission time can be expected, and measuring the exciton radiative lifetime is thus crucial. TRPL is the ideal spectroscopy tool for such a measurement. In our previous works, we measured low-temperature PL decay times of 4 ps for MoS₂ MLs [54] and 2 ps for MoSe₂ and WSe₂ MLs [66]. Our temperature-dependent study on a MoSe₂ ML suggested that this decay time corresponds to the radiative lifetime of excitons before thermalization occurs. In Fig. 4, we present the low-temperature PL dynamics of X_A^{1s} for both MoTe₂ MLs and BLs. The excitation wavelength of 850 nm (1.458 eV) is chosen to match with the enhanced absorption at the X_B^{1s} exciton transition [see Fig. 3(a)]. For the ML, we observe a monoexponential decay that can be fitted with a characteristic time of $\tau^{\text{ML}} \sim 3.4 \pm 0.5$ ps. This dynamic is clearly longer than the time resolution of our setup measured by detecting the laser pulse backscattered from the sample on the streak camera (shaded area). Following Ref. [66], we interpret this fast decay time as the radiative lifetime of the excitons. A key argument is that the X_A^{1s} PL intensity is constant in the range of 10–40 K [see Fig. 2(b)] excluding any role of nonradiative channels at low temperatures. In the context of the optical generation of valley polarization, the short PL emission time τ^{ML} of 3.4 ps implies that either the valley depolarization

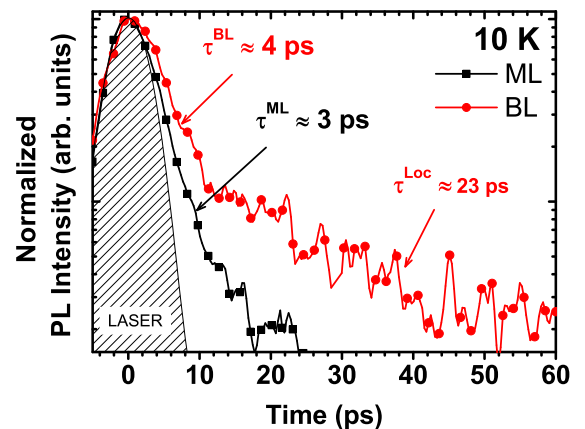


FIG. 4. Time-resolved photoluminescence of the neutral exciton X_A^{1s} in the MoTe₂ ML (black) and BL (red) following a resonant excitation on the B exciton [$E_{\text{laser}} = 1.458$ eV (850 nm)] at 10 K. The instrument response is obtained by detecting the backscattered laser pulse on the sample surface, see the hatched area labeled “LASER.”

time is considerably shorter than 3.4 ps or the initially created valley polarization is negligible. For the BL, the decay is biexponential. We attribute the longest decay time (23 ps) to the presence of localized states at the same energy as the free exciton peak. The shortest decay time $\tau^{\text{BL}} \sim 4.3 \pm 0.5$ ps can be attributed to the lifetime of free excitons in the BL. It is thus very similar to τ^{ML} and six times faster than for the indirect transition in a WSe₂ BL [67]. This suggests a direct transition in a MoTe₂ BL in agreement with the reflectivity spectra of Fig. 3(b). Nevertheless, we want to point out that contrary to the ML, the PL intensity of the BL decreases as soon as the temperature is raised. We thus cannot exclude that this decay time is also governed by nonradiative recombination. Interestingly, this time is slightly longer than τ^{ML} , which might hint at the fact that the radiative lifetime of excitons in the BL is longer than the radiative lifetime of excitons in the ML. Several hypotheses can be proposed at this stage. Even if the PL of a MoTe₂ BL originates from a direct transition, it was reported that the optical band gap of a MoTe₂ BL may be borderline direct/indirect [27,28]. It is thus not surprising to observe a smaller rate of radiative recombination in the BL. Second, potential fluctuations with a high spatial frequency have been proposed to explain the significant discrepancy between the measured exciton lifetime (a few picoseconds) and the theoretical radiative lifetime of free excitons (a few hundreds of femtoseconds) [66]. We expect larger Bohr radius excitons in the BLs to be more sensitive to these fluctuations than smaller Bohr radius excitons in the ML and consequently to yield longer radiative lifetimes.

V. EXCITON-EXCITON ANNIHILATION

Nonradiative recombination channels are known to play a major role in the poor luminescence yield measured at room temperature in TMD MLs [68]. In addition to defect-related recombination, EEA is known to be very efficient in MoS₂, MoSe₂, WS₂, and WSe₂ at room temperature even for moderate excitation power density [68,69]. In Fig. 5, we plot the variations of the X_A^{1s} PL intensity as a function of excitation power for both the ML and the BL at 10 and 200 K. For the ML, the X_A^{1s} PL intensity scales linearly at 10 K whereas it scales sublinearly ($\sim P^{0.8}$) at 200 K for excitation powers larger than 10 μW . This might be a consequence of the thermal activation of EEA processes. At 10 K, the exciton diffusion is too small, and the radiative lifetime is so short that EEA does not compete with radiative recombination. In contrast, when the temperature increases, the mobility of the excitons increases [69,70] and so does the effective radiative lifetime of the excitons due to thermalization [22,71,72]. This enhances the sensitivity to many-body interactions. Remarkably, for the BL, the situation is different. As shown in Fig. 5, the X_A^{1s} PL intensity increases linearly with the excitation power for both temperatures suggesting a reduced EEA rate as compared to the ML. We also observe the linearity at room temperature (not shown here). Such a property combined with an efficient optical transition would make the MoTe₂ BL a very promising candidate for optoelectronics applications requiring high carrier densities including laser or concentrating solar cells [73]. Unfortunately, a clear conclusion cannot be drawn at this stage. First, we notice that, at 10 K, the PL intensities of

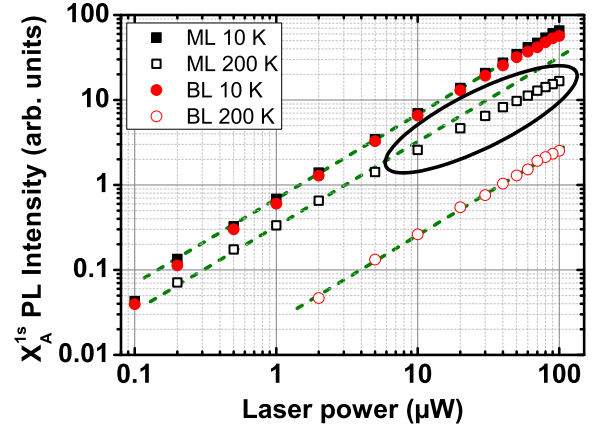


FIG. 5. Dependence of the X_A^{1s} PL intensity with the laser power in the MoTe₂ ML (black square points) and BL (red circles points) at 10 K (filled symbols) and 200 K (opened symbols). The sample is excited with a cw HeNe laser (633 nm). The green dashed lines indicate linear slopes. The black circle highlights the nonlinear dependence of the X_A^{1s} PL intensity in the MoTe₂ ML at 200 K. With our estimated spot size and assuming an absorption of 10%, a power of 100 μW is equivalent to a density of absorbed photons of $4.10^{21} \text{ cm}^{-2} \text{ s}^{-1}$.

the MLs and BLs are on the same order of magnitude whereas at 200 K, the BL intensity is one order of magnitude lower than the ML intensity (for the same excitation power). This could be due to a higher defect density in the BL. Passivation capping or chemical treatments [68,74,75] would help to study the real influence of defects on the optical properties of the MoTe₂ ML and BL. A second explanation would be that the indirect transition plays a more important role at elevated temperatures (due to thermal activation or direct-to-indirect crossover). Actually, Yuan and Huang already measured the EEA rates in the WS₂ ML and BL [76] and found a rate for the BL two orders of magnitude lower than in the ML due to the reduced phonon-assisted EEA of indirect excitons in the indirect band gap WS₂ BL. Thus, we can expect a similar behavior if the MoTe₂ BL is indirect at elevated temperatures. Finally, we cannot exclude that the mobility of excitons is reduced in the MoTe₂ BL, which could explain why the EEA processes are not visible even at high temperatures.

In conclusion, we studied the optical properties of the MoTe₂ ML and BL. We performed DFT-GW calculations and found a direct electronic band gap for the ML and an indirect one for the BL. With one-photon PLE and reflectivity, we found that the energy of the B -exciton state is the same in the ML and the BL in agreement with the BSE calculations. We did not find a clear signature of the X_A^{2s} exciton excited state which may lie close to the X_B^{1s} resonance. We did not detect any circular or linear PL polarization for laser energy as close as 60 meV above the energy of the X_A^{1s} exciton. We measured the exciton lifetimes of the ML and the BL at low temperatures. The lifetime in the BL is slightly longer than the radiative lifetime in the ML but remains significantly faster than for the BLs of other TMD materials. Combined with the observation of similar oscillator strength for X_A^{1s} in the ML and the BL in reflectivity measurements, we can reasonably argue that the low-temperature PL originates from direct transitions in both

MLs and BLs. Finally, we discussed the observed reduction of the EEA contribution to the nonradiative recombination in the MoTe₂ BL.

ACKNOWLEDGMENTS

We thank the ANR MoS₂ Valley Control and Programme Investissements d’Avenir Grant No. ANR-11-IDEX-0002-02, reference Grant No. ANR-10-LABX-0037-NEXT, and ERC

Grant No. 306719 for financial support. A.H. acknowledges ERC Grant No. 336749. I.C.G. also acknowledges the CALMIP initiative for the generous allocation of computational times, through Project No. p0812 as well as the GENCI-CINES, GENCI-IDRIS, and GENCI-CCRT for Grant No. x2016096649. I.C.G. thanks the CNRS for financial support. X.M. also acknowledges the Institut Universitaire de France.

-
- [1] B. Radisavljevic, A. Radenovic, J. Brivio, V. Giacometti, and A. Kis, *Nat. Nanotechnol.* **6**, 147 (2011).
- [2] O. Lopez-Sanchez, D. Lembke, M. Kayci, A. Radenovic, and A. Kis, *Nat. Nanotechnol.* **8**, 497 (2013).
- [3] J. S. Ross, P. Klement, A. M. Jones, N. J. Ghimire, J. Yan, D. G. Mandrus, T. Taniguchi, K. Watanabe, K. Kitamura, W. Yao, D. H. Cobden, and X. Xu, *Nat. Nanotechnol.* **9**, 268 (2014).
- [4] F. Withers, O. Del Pozo-Zamudio, A. Mishchenko, A. P. Rooney, A. Gholinia, K. Watanabe, T. Taniguchi, S. J. Haigh, A. K. Geim, A. I. Tartakovskii, and K. S. Novoselov, *Nature Mater.* **14**, 301 (2015).
- [5] K. F. Mak, C. Lee, J. Hone, J. Shan, and T. F. Heinz, *Phys. Rev. Lett.* **105**, 136805 (2010).
- [6] A. Splendiani, L. Sun, Y. Zhang, T. Li, J. Kim, C.-Y. Chim, G. Galli, and F. Wang, *Nano Lett.* **10**, 1271 (2010).
- [7] S. Tongay, J. Zhou, C. Ataca, K. Lo, T. S. Matthews, J. Li, J. C. Grossman, and J. Wu, *Nano Lett.* **12**, 5576 (2012).
- [8] W. Zhao, Z. Ghorannevis, L. Chu, M. Toh, C. Kloc, P.-H. Tan, and G. Eda, *ACS Nano* **7**, 791 (2013).
- [9] Y. Chen, J. Xi, D. O. Dumcenco, Z. Liu, K. Suenaga, D. Wang, Z. Shuai, Y.-S. Huang, and L. Xie, *ACS Nano* **7**, 4610 (2013).
- [10] S. Tongay, D. S. Narang, J. Kang, W. Fan, C. Ko, A. V. Luce, K. X. Wang, J. Suh, K. D. Patel, V. M. Pathak, J. Li, and J. Wu, *Appl. Phys. Lett.* **104**, 12101 (2014).
- [11] G. Wang, C. Robert, A. Suslu, B. Chen, S. Yang, S. Alamdari, I. C. Gerber, T. Amand, X. Marie, S. Tongay, and B. Urbaszek, *Nat. Commun.* **6**, 10110 (2015).
- [12] Z. Ye, T. Cao, K. O’Brien, H. Zhu, X. Yin, Y. Wang, S. G. Louie, and X. Zhang, *Nature (London)* **513**, 214 (2014).
- [13] A. Chernikov, T. C. Berkelbach, H. M. Hill, A. Rigosi, Y. Li, O. B. Aslan, D. R. Reichman, M. S. Hybertsen, and T. F. Heinz, *Phys. Rev. Lett.* **113**, 076802 (2014).
- [14] G. Wang, X. Marie, I. Gerber, T. Amand, D. Lagarde, L. Bouet, M. Vidal, A. Balocchi, and B. Urbaszek, *Phys. Rev. Lett.* **114**, 097403 (2015).
- [15] D. Xiao, G.-B. Liu, W. Feng, X. Xu, and W. Yao, *Phys. Rev. Lett.* **108**, 196802 (2012).
- [16] T. Cao, G. Wang, W. Han, H. Ye, C. Zhu, J. Shi, Q. Niu, P. Tan, E. Wang, B. Liu, and J. Feng, *Nat. Commun.* **3**, 887 (2012).
- [17] K. F. Mak, K. He, J. Shan, and T. F. Heinz, *Nat. Nanotechnol.* **7**, 494 (2012).
- [18] G. Sallen, L. Bouet, X. Marie, G. Wang, C. R. Zhu, W. P. Han, Y. Lu, P. H. Tan, T. Amand, B. L. Liu, and B. Urbaszek, *Phys. Rev. B* **86**, 081301(R) (2012).
- [19] L. Yang, N. A. Sinitsyn, W. Chen, J. Yuan, J. Zhang, J. Lou, and S. A. Crooker, *Nat. Phys.* **11**, 830 (2015).
- [20] J. P. Echeverry, B. Urbaszek, T. Amand, X. Marie, and I. C. Gerber, *Phys. Rev. B* **93**, 121107 (2016).
- [21] F. Withers, O. Del Pozo-Zamudio, S. Schwarz, S. Dufferwiel, P. M. Walker, T. Godde, A. P. Rooney, A. Gholinia, C. R. Woods, P. Blake, S. J. Haigh, K. Watanabe, T. Taniguchi, I. L. Aleiner, A. K. Geim, V. I. Fal’ko, A. I. Tartakovskii, and K. S. Novoselov, *Nano Lett.* **15**, 8223 (2015).
- [22] X.-X. Zhang, Y. You, S. Y. Frank Zhao, and T. F. Heinz, *Phys. Rev. Lett.* **115**, 257403 (2015).
- [23] G. Wang, E. Palleau, T. Amand, S. Tongay, X. Marie, and B. Urbaszek, *Appl. Phys. Lett.* **106**, 112101 (2015).
- [24] G. Kioseoglou, A. T. Hanbicki, M. Currie, A. L. Friedman, and B. T. Jonker, *Sci. Rep.* **6**, 25041 (2016).
- [25] J. Xiao, Z. Ye, Y. Wang, H. Zhu, Y. Wang, and X. Zhang, *Light: Sci. Appl.* **4**, e366 (2015).
- [26] C. Ruppert, O. B. Aslan, and T. F. Heinz, *Nano Lett.* **14**, 6231 (2014).
- [27] I. G. Lezama, A. Arora, A. Ubaldini, C. Barreateau, E. Giannini, M. Potemski, and A. F. Morpurgo, *Nano Lett.* **15**, 2336 (2015).
- [28] G. Froehlicher, E. Lorchat, and S. Berciaud, *Phys. Rev. B* **94**, 085429 (2016).
- [29] A. Ramasubramaniam, *Phys. Rev. B* **86**, 115409 (2012).
- [30] H.-P. Komsa and A. V. Krasheninnikov, *Phys. Rev. B* **88**, 085318 (2013).
- [31] A. Molina-Sánchez, D. Sangalli, K. Hummer, A. Marini, and L. Wirtz, *Phys. Rev. B* **88**, 045412 (2013).
- [32] D. Y. Qiu, F. H. da Jornada, and S. G. Louie, *Phys. Rev. Lett.* **111**, 216805 (2013).
- [33] G. Kresse and J. Hafner, *Phys. Rev. B* **47**, 558 (1993).
- [34] G. Kresse and J. Furthmüller, *Comput. Mater. Sci.* **6**, 15 (1996).
- [35] P. E. Blöchl, *Phys. Rev. B* **50**, 17953 (1994).
- [36] G. Kresse and D. Joubert, *Phys. Rev. B* **59**, 1758 (1999).
- [37] J. Heyd and G. E. Scuseria, *J. Chem. Phys.* **120**, 7274 (2004).
- [38] J. Heyd, J. E. Peralta, G. E. Scuseria, and R. L. Martin, *J. Chem. Phys.* **123**, 174101 (2005).
- [39] J. Paier, M. Marsman, K. Hummer, G. Kresse, I. C. Gerber, and J. G. Ángyán, *J. Chem. Phys.* **124**, 154709 (2006).
- [40] M. Shishkin and G. Kresse, *Phys. Rev. B* **74**, 035101 (2006).
- [41] J. He, K. Hummer, and C. Franchini, *Phys. Rev. B* **89**, 075409 (2014).
- [42] J. Klimeš, D. R. Bowler, and A. Michaelides, *J. Phys.: Condens. Matter* **22**, 022201 (2010).
- [43] A. A. Mostofi, J. R. Yates, Y.-S. Lee, I. Souza, D. Vanderbilt, and N. Marzari, *Comput. Phys. Commun.* **178**, 685 (2008).
- [44] J. Yang, T. Lü, Y. W. Myint, J. Pei, D. MacDonald, J.-C. Zheng, and Y. Lu, *ACS Nano* **9**, 6603 (2015).

- [45] A. Molina-Sánchez, M. Palumbo, A. Marini, and L. Wirtz, *Phys. Rev. B* **93**, 155435 (2016).
- [46] H.-P. Komsa and A. V. Krasheninnikov, *Phys. Rev. B* **86**, 241201 (2012).
- [47] B. Davey and B. L. Evans, *Phys. Status Solidi A* **13**, 483 (1972).
- [48] A. Castellanos-Gomez, M. Buscema, R. Molenaar, V. Singh, L. Janssen, H. S. J. van der Zant, and G. A. Steele, *2D Mater.* **1**, 11002 (2014).
- [49] A. M. Jones, H. Yu, J. R. Schaibley, J. Yan, D. G. Mandrus, T. Taniguchi, K. Watanabe, H. Dery, W. Yao, and X. Xu, *Nat. Phys.* **12**, 323 (2016).
- [50] F. Cadiz, S. Tricard, M. Gay, D. Lagarde, G. Wang, C. Robert, P. Renucci, B. Urbaszek, and X. Marie, *Appl. Phys. Lett.* **108**, 251106 (2016).
- [51] J. R. Bindel, M. Pezzotta, J. Ulrich, M. Liebmann, E. Y. Sherman, and M. Morgenstern, *Nat. Phys.* **12**, 920 (2016).
- [52] M. M. Glazov, E. Y. Sherman, and V. K. Dugaev, *Physica E* **42**, 2157 (2010).
- [53] G. Kioseoglou, A. T. Hanbicki, M. Currie, A. L. Friedman, D. Gunlycke, and B. T. Jonker, *Appl. Phys. Lett.* **101**, 221907 (2012).
- [54] D. Lagarde, L. Bouet, X. Marie, C. R. Zhu, B. L. Liu, T. Amand, P. H. Tan, and B. Urbaszek, *Phys. Rev. Lett.* **112**, 047401 (2014).
- [55] G. Wang, M. M. Glazov, C. Robert, T. Amand, X. Marie, and B. Urbaszek, *Phys. Rev. Lett.* **115**, 117401 (2015).
- [56] G. Wang, I. C. Gerber, L. Bouet, D. Lagarde, A. Balocchi, M. Vidal, T. Amand, X. Marie, and B. Urbaszek, *2D Mater.* **2**, 45005 (2015).
- [57] D. Kozawa, R. Kumar, A. Carvalho, K. Kumar Amara, W. Zhao, S. Wang, M. Toh, R. M. Ribeiro, A. H. Castro Neto, K. Matsuda, and G. Eda, *Nat. Commun.* **5**, 4543 (2014).
- [58] H. M. Hill, A. F. Rigosi, C. Roquelet, A. Chernikov, T. C. Berkelbach, D. R. Reichman, M. S. Hybertsen, L. E. Brus, and T. F. Heinz, *Nano Lett.* **15**, 2992 (2015).
- [59] K. F. Mak, M. Y. Sfeir, Y. Wu, C. H. Lui, J. A. Misewich, and T. F. Heinz, *Phys. Rev. Lett.* **101**, 196405 (2008).
- [60] A. Arora, R. Schmidt, R. Schneider, M. R. Molas, I. Breslavetz, M. Potemski, and R. Bratschitsch, *Nano Lett.* **16**, 3624 (2016).
- [61] A. Molina-Sánchez and L. Wirtz, *Phys. Rev. B* **84**, 155413 (2011).
- [62] S. Horzum, H. Sahin, S. Cahangirov, P. Cudazzo, A. Rubio, T. Serin, and F. M. Peeters, *Phys. Rev. B* **87**, 125415 (2013).
- [63] H. Guo, T. Yang, M. Yamamoto, L. Zhou, R. Ishikawa, K. Ueno, K. Tsukagoshi, Z. Zhang, M. S. Dresselhaus, and R. Saito, *Phys. Rev. B* **91**, 205415 (2015).
- [64] S. Dufferwiel, S. Schwarz, F. Withers, A. A. P. Trichet, F. Li, M. Sich, O. Del Pozo-Zamudio, C. Clark, A. Nalitov, D. D. Solnyshkov, G. Malpuech, K. S. Novoselov, J. M. Smith, M. S. Skolnick, D. N. Krizhanovskii, and A. I. Tartakovskii, *Nat. Commun.* **6**, 8579 (2015).
- [65] X. Liu, T. Galfsky, Z. Sun, F. Xia, E. Lin, Y.-H. Lee, S. Kéna-Cohen, and V. M. Menon, *Nat. Photonics* **9**, 30 (2015).
- [66] C. Robert, D. Lagarde, F. Cadiz, G. Wang, B. Lassagne, T. Amand, A. Balocchi, P. Renucci, S. Tongay, B. Urbaszek, and X. Marie, *Phys. Rev. B* **93**, 205423 (2016).
- [67] G. Wang, X. Marie, L. Bouet, M. Vidal, A. Balocchi, T. Amand, D. Lagarde, and B. Urbaszek, *Appl. Phys. Lett.* **105**, 182105 (2014).
- [68] M. Amani, D.-H. Lien, D. Kiriya, J. Xiao, A. Azcatl, J. Noh, S. R. Madhupathy, R. Addou, S. KC, M. Dubey, K. Cho, R. M. Wallace, S.-C. Lee, J.-H. He, J. W. Ager, III, X. Zhang, E. Yablonovitch, and A. Javey, *Science* **350**, 1065 (2015).
- [69] Y. Yu, Y. Yu, C. Xu, A. Barrette, K. Gundogdu, and L. Cao, *Phys. Rev. B* **93**, 201111(R) (2016).
- [70] S. Mouri, Y. Miyauchi, M. Toh, W. Zhao, G. Eda, and K. Matsuda, *Phys. Rev. B* **90**, 155449 (2014).
- [71] T. Korn, S. Heydrich, M. Hirmer, J. Schmutzler, and C. Schüller, *Appl. Phys. Lett.* **99**, 102109 (2011).
- [72] T. Yan, X. Qiao, X. Liu, P. Tan, and X. Zhang, *Appl. Phys. Lett.* **105**, 101901 (2014).
- [73] O. Salehzadeh, M. Djavid, N. H. Tran, I. Shih, and Z. Mi, *Nano Lett.* **15**, 5302 (2015).
- [74] M. Amani, P. Taheri, R. Addou, G. H. Ahn, D. Kiriya, D.-H. Lien, J. W. Ager, R. M. Wallace, and A. Javey, *Nano Lett.* **16**, 2786 (2016).
- [75] H.-V. Han, A.-Y. Lu, L.-S. Lu, J.-K. Huang, H. Li, C.-L. Hsu, Y.-C. Lin, M.-H. Chiu, K. Suenaga, C.-W. Chu, H.-C. Kuo, W.-H. Chang, L.-J. Li, and Y. Shi, *ACS Nano* **10**, 1454 (2016).
- [76] L. Yuan and L. Huang, *Nanoscale* **7**, 7402 (2015).